Available online at www.sciencedirect.com
ScienceDirect
Geochimica et Cosmochimica Acta 73 (2009) 3277–3290
Geochimica et Cosmochimica Acta
www.elsevier.com/locate/gca

Pyrite oxidation during sample storage determines phosphorus fractionation in carbonate-poor anoxic sediments

Peter Kraal [a,*], Caroline P. Slomp [a], Astrid Forster [b,1], Marcel M.M. Kuypers [c], Appy Sluijs [d]

[a] Department of Earth Sciences – Geochemistry, Faculty of Geosciences, Budapestlaan 4, 3584 CD Utrecht, The Netherlands
[b] Department of Marine Biogeochemistry and Toxicology, Royal Netherlands Institute for Sea Research, P.O. Box 59, 1790 AB Den Burg, Texel, The Netherlands
[c] Nutrient Group, Max Planck Institute for Marine Microbiology, Celsiusstr. 1, D-28359, Bremen, Germany
[d] Department of Biology – Palaeoecology, Institute of Environmental Biology, Utrecht University, Budapestlaan 4, 3584 CD, The Netherlands

Received 17 June 2008; accepted in revised form 27 February 2009; available online 6 March 2009

Abstract

We investigated the phosphorus (P) and iron (Fe) fractionation in four cores with anoxic sediments, deposited during the mid-Cretaceous oceanic anoxic event 2 (~94 Ma) and the Paleocene–Eocene thermal maximum (~55 Ma), that were exposed to oxygen after core recovery. Surprisingly, P associated with iron oxyhydroxides (Fe-bound P) was a major P phase in these laminated sediments deposited under euxinic conditions. A significant fraction of total Fe was present as (poorly) crystalline ferric Fe. This fraction increased with increasing storage time of the investigated cores. In carbonate-poor samples, Fe-bound P accounted for up to 99% of total P and its abundance correlated with pyrite contents. In samples with higher $CaCO_3$ contents (>5 wt% in the investigated samples), P was mostly present in authigenic Ca–P minerals, irrespective of pyrite contents. We conclude that the P fractionation in anoxic, carbonate-poor, sediments is strongly affected by pyrite oxidation that occurs when these sediments are exposed to oxygen. Pyrite oxidation produces sulfuric acid and iron oxyhydroxides. The abundance of poorly crystalline Fe oxyhydroxides provides further evidence that these were indeed formed through recent (post-recovery) oxidation rather than in situ tens of millions of years ago. The acid dissolves apatite and the released phosphate is subsequently bound in the freshly formed iron oxyhydroxides. Pyrite oxidation thus leads to a conversion of authigenic Ca–P to Fe-bound P. In more calcareous samples, $CaCO_3$ can act as an effective buffer against acidic dissolution of Ca–P minerals. The results indicate that shielding of sediments from atmospheric oxygen is vital to preserve the in situ P fractionation and to enable a valid reconstruction of marine phosphorus cycling based on sediment records.

1. INTRODUCTION

Phosphorus (P) is an essential nutrient that can limit marine primary productivity, especially on geological timescales (Holland, 1978; Tyrrell, 1999). This relationship makes the mechanisms and efficiency of P burial of great biogeochemical importance. In particular, the enhanced release of P from sediments that were exposed to conditions of prolonged bottom water anoxia has been suggested as an important factor in sustaining periods of ocean anoxia in Earth's past (Ingall and Jahnke, 1994; Van Cappellen and Ingall, 1994; Mort et al., 2007). To gain further insight in the mechanisms of P burial and regeneration, the identification of the different P phases in sediments and their response to changes in bottom water oxygenation is a major objective. Chemical extraction techniques have been developed to differentiate between iron oxide-bound, authigenic, biogenic, detrital and organic P reservoirs (e.g. Lucotte and D'anglejan, 1985; Ruttenberg, 1992; Schenau and De

* Corresponding author.
E-mail address: p.kraal@geo.uu.nl (P. Kraal).
[1] Present address: Rommelstr. 34, 49809 Lingen, Germany.

0016-7037/$ - see front matter © 2009 Elsevier Ltd. All rights reserved.
doi:10.1016/j.gca.2009.02.026

Lange, 2000). Sediment P fractionation has been used to investigate P cycling and burial mechanisms, up to the global scale (Ruttenberg, 1993; Filippelli, 2001). Furthermore, changes in marine sediment P abundance and fractionation with depth in (ancient) sediments have been linked to variations in the oxygenation state of bottom waters over time (Slomp et al., 2002; Tamburini et al., 2002; Mort et al., 2007; März et al., 2008).

However, anoxic sediments are sensitive to chemical alterations when brought into contact with oxygen (Wiggering, 1993; Ohtsubo, 1995; Peterson et al., 1996), which often occurs during core recovery and sample processing. The altered sediment chemistry may then no longer reflect in situ bottom waters conditions. While interest in sediment P fractionation is enormous, little is known about the changes in P fractionation in reduced sediments exposed to oxygen during storage and processing. In particular, oxidation of pyrite with oxygen is of relevance, given that the sulfuric acid produced in this reaction can dissolve P-bearing Ca-minerals (Chi et al., 2006). Oxidation of pyrite was recently suggested as one of the possible mechanisms causing an increase of P bound to reducible Fe and a decrease of Ca-bound P in anoxic Baltic Sea sediments exposed to atmospheric oxygen for ca. 3 months (Lukkari et al., 2007).

Even though it is known that anoxic sediments are sensitive to oxygen, it is still common practice to store sediment samples exposed to oxygen. Here, we (i) investigate how oxygen exposure has affected the P fractionation in ancient sediments that originally formed under anoxic conditions and (ii) establish relationships between P fractionation and various chemical sediment characteristics (Fe, S and $CaCO_3$ contents).

We used sediments recovered during Deep Sea Drilling Project (DSDP) and (Integrated) Ocean Drilling Program ((I)ODP) expeditions that were deposited during the mid-Cretaceous Cenomanian–Turonian oceanic anoxic event (OAE 2, ~93.55 Ma: Schlanger and Jenkyns, 1976; Sageman et al., 2006) and during the Paleocene–Eocene thermal maximum (PETM, ~55 Ma: Zachos et al., 1993; Sluijs et al., 2007). The results indicate that shielding of sediments from atmospheric oxygen is vital to enable a valid reconstruction of marine phosphorus cycling and in situ bottom water conditions based on P fractionation in sediment records.

2. MATERIALS AND METHODS

2.1. Provenance and treatment of sediments

The Late-Cretaceous OAE 2 samples were recovered during DSDP Leg 41 in 1975 (Site 367: Cape Verde Basin off-shore Senegal, eastern equatorial Atlantic; Lancelot et al., 1977), DSDP Leg 93 in 1983 (Site 603, Hole B: lower continental rise, North American Basin, NW-Atlantic; Van Hinte et al., 1984) and ODP Leg 207 in 2003 (Site 1260: Demerara Rise, off-shore Suriname and French Guyana, western equatorial Atlantic; Erbacher et al., 2004). The PETM samples were drilled during IODP Expedition 302 in 2004 (Site M004A, Lomonosov Ridge, central Arctic Ocean; Backman et al., 2006).

Sediment cores from Leg 207 and Leg 302 were kept in plastic tubes without shielding from oxygen at 4 °C in the IODP Core Repository at Bremen University, Germany. Cores from Leg 41 and 93 were stored under similar conditions at the Lamont–Doherty Earth Observatory in Palisades, NY, USA. The cores from sites 367 and 603 were sampled in 1997/1998, those from Site 1260 in 2003/2004 and the cores from Site M004A in 2006. The sediments have thus been exposed to atmospheric oxygen for years (storage time: Site 367 > Site 603 >> Site 1260 > Site M004A). Splits of the samples that were freeze-dried and ground shortly after sampling were used for the P extractions presented in this paper (performed in 2007 and 2008).

2.2. Depositional environment

2.2.1. OAE 2 Samples (sites 367, 603 and 1260)

The OAE 2 sediments of sites 367 and 603 were deposited in a deep sea environment below the carbonate compensation depth (Lancelot et al., 1977; Van Hinte et al., 1984). Consequently, samples of Site 603 are low in $CaCO_3$ (<2 wt%). Sediments of Site 367 are generally also low in $CaCO_3$ (<2 wt%) but contain several $CaCO_3$-rich (10–20 wt%) layers that were probably formed by sediment input from the adjacent continental margin (Lancelot et al., 1977). The investigated samples of sites 367 and 603, which cover the early to middle stages of OAE 2 (Kuypers et al., 2002; Kuypers et al., 2004a), consist of laminated black shales (Site 367) and alternating black carbonaceous and pelagic greenish grey claystones (Site 603). During OAE 2, Site 1260 was located in a slope environment at intermediate water depth. The OAE 2 interval consists of $CaCO_3$-rich laminated black shales (Erbacher et al., 2004).

Sediments of all three sites contain visible pyrite and display features indicative of euxinic conditions during deposition of (part of the) investigated OAE 2 interval such as lamination and enrichment in redox-sensitive trace metals that are immobilized under reducing conditions. High organic carbon (C_{org}) contents (up to 40 wt%), lamination and high concentrations of redox-sensitive trace metals such as Mo, Ni, V and Zn are found throughout the investigated profile from Site 367 (Kuypers et al., 2002). The sampled OAE 2 interval of Site 603 contains distinct laminated organic-rich black claystones with C_{org} contents >1 wt% that are enriched in redox-sensitive trace metals, alternating with C_{org}-poor (<1 wt%) green claystones that were deposited under more oxygenated conditions (Kuypers et al., 2004a). Two of these distinct laminated organic-rich black claystone layers were sampled in detail (see Fig. 1b). The OAE 2 interval at Site 1260 consists of laminated black shales (Erbacher et al., 2004). Both micropalaeontological and geochemical evidence indicate that the investigated sediments were deposited under bottom waters that experienced prolonged oxygen depletion during OAE 2 (Brumsack, 2006; Friedrich and Erbacher, 2006). Also, the investigated laminated sections of sites 367 and 603 contain derivatives of the pigment isorenieratene (Kuypers et al., 2002; Kuypers et al., 2004b). These compounds are derived from the brown strain of photosynthetic green sulfur bacteria, which requires euxinic (anoxic and sulphidic) condi-

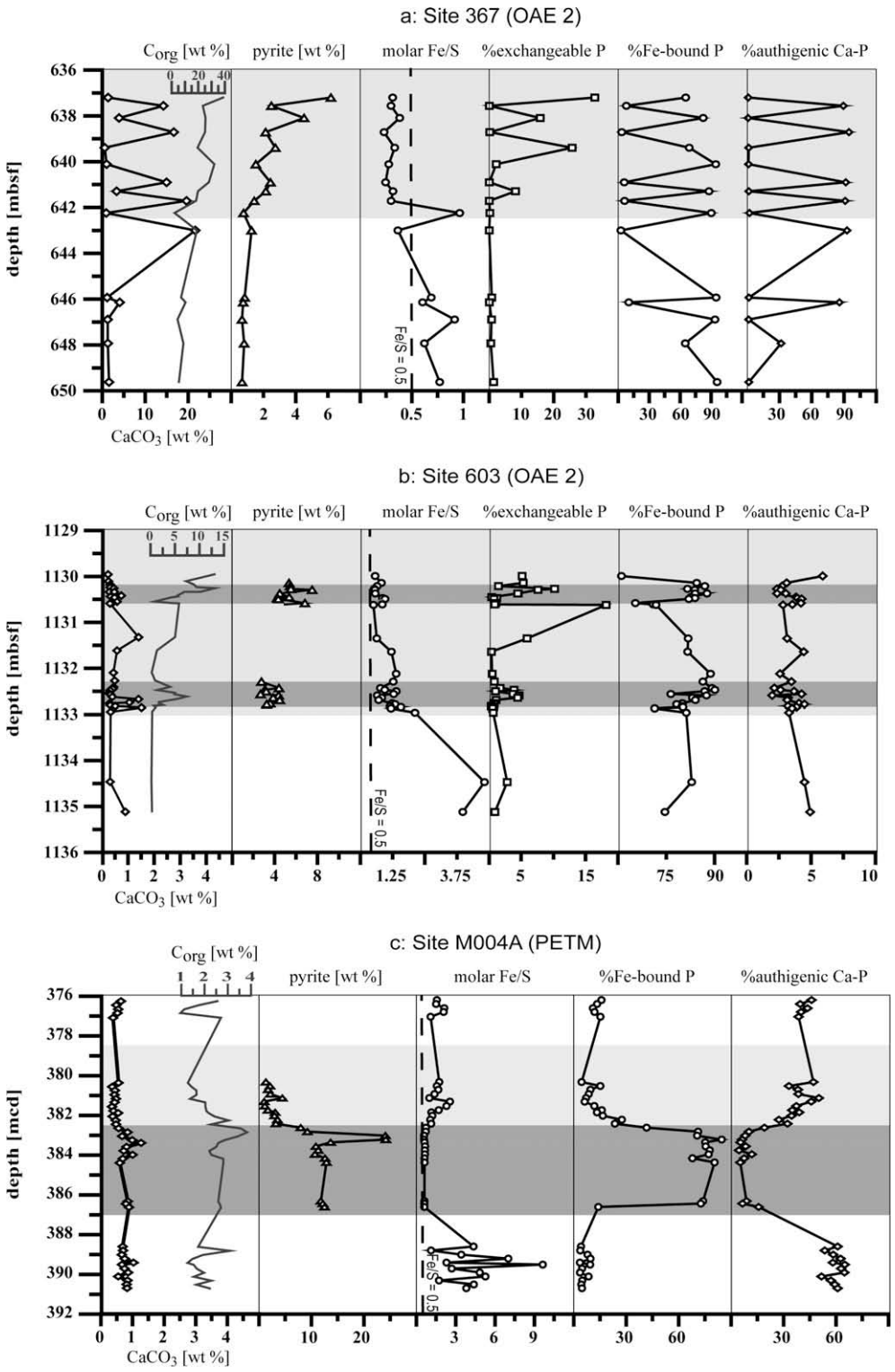

Fig. 1. $CaCO_3$, C_{org}, and pyrite contents, molar total Fe/total S ratio and major P phases as percentage of total P for sites 367 (a), 603 (b) and M004A (c). Exchangeable P was not determined in M004A samples. Light grey areas indicate the OAE 2 or PETM intervals. The darker grey areas in (b) indicate the laminated, organic-rich black claystone layers within the OAE 2 interval of Site 603 that were investigated at high resolution. Pyrite content was only calculated for these black claystone layers. The dark grey area in (c) represents the organic-rich laminated sediments deposited under euxinic conditions during the lower part of the PETM interval. Pyrite content was only calculated for the PETM interval of Site M004A. The black dotted line indicates molar Fe/S = 0.5 which is the stoichiometric boundary between Fe (Fe/S < 0.5) or S (Fe/S > 0.5) limitation with respect to pyrite formation. Depth is given in meters below sea floor (mbsf) or meters composite depth (mcd).

tions to thrive (Sinninghe Damsté et al., 1993; Imhoff, 1995).

2.2.2. PETM Samples (Site M004A)

The PETM interval is part of a sequence of upper Paleocene to lower Eocene organic-rich siliciclastic claystones (Backman et al., 2006). The samples of the PETM interval are $CaCO_3$-poor (<2 wt%), which is likely the result of carbonate dissolution in the water column and in the sediment. The sediments in the lower part of the PETM interval (up to 382.5 mcd) contain visible pyrite and are laminated, containing 1–4 wt% C_{org}. Moreover, these sediments are enriched in redox-sensitive trace metals such as As, Mo, U and V that are indicative of bottom water anoxia (Sluijs et al., 2008). This lower part also contains detectable levels of isorenieratene (Sluijs et al., 2006).

2.3. Sediment P and Fe fractionation

For the solid phase P fractionation, we used the sequential chemical extraction (SEDEX) procedure developed by Ruttenberg (1992) as modified by Slomp et al. (1996a). The SEDEX procedure separates total sediment P into exchangeable P and P associated with: iron oxyhydroxides (Fe-bound P); $CaCO_3$, authigenic and biogenic calcium minerals (authigenic Ca–P); detrital material (detrital P) and organic matter (organic P). The extractions were performed at room temperature (22 °C).

Exchangeable P was determined by extraction with 1 M $MgCl_2$ (pH 8, 0.5 h). An extraction with citrate–dithionite bicarbonate (CDB, pH 7.3, 8 h) and a subsequent 1 M $MgCl_2$ (pH 8, 0.5 h) wash step followed to extract P (and Fe) associated with iron oxyhydroxides (Fe-bound P). The sediment residue was then treated with a Na-acetate buffer (pH 4, 6 h) and again 1 M $MgCl_2$ (pH 8, 0.5 h) to extract authigenic Ca–P. Remaining inorganic (i.e. detrital) P was subsequently extracted with 1 M HCl (24 h). Finally, organic P was obtained by combusting the sediment residue at 550 °C (2 h) and extracting the P released from organic matter with 1 M HCl (24 h). No separate exchangeable P extraction step was applied to the M004A (PETM) samples (any exchangeable P was thus extracted during the CDB step).

A separate series of samples of sites M004A (PETM) and 367 (OAE 2) was treated with a solution of 50 g/L Na-citrate, 50 g/L Na-bicarbonate and 20 g/L L(+)-ascorbic acid (CBA) to extract Fe and P associated with poorly crystalline iron oxyhydroxides (Hyacinthe et al., 2006).

Phosphorus and Fe concentrations in the CDB extracts were measured with Inductively Coupled Plasma-Optical Emission Spectroscopy (ICP-OES: Perkin Elmer Optima 3000). Phosphorus concentrations in all other extracts were determined with the colorimetric method of Strickland and Parsons (1972) on a Shimadzu Spectrophotometer. Total extracted Fe concentrations in the CBA extracts were determined with the colorimetric method of Stookey (1970). Duplicates and internal standards were included in the extraction series to assure accuracy and reproducibility. Relative standard deviations for duplicates and in-house standards were <5%. The relative standard deviation for P in the CDB samples was higher, up to 15%. Molar Fe/P ratios in CDB and CBA extracts were used as indicators of the nature of the iron oxyhydroxides with low Fe/P ratios around 10 being suggestive of P scavenging by relatively fresh (amorphous) iron oxyhydroxides (Slomp et al., 1996b; Anschutz et al., 1998). The P concentrations in the CBA extracts from some samples were close to the detection limit. Relative standard deviations were significant (up to 30%) and the Fe/P ratios in the CBA extracts should thus be treated as indicative values.

2.4. $CaCO_3$ and FeS_2 contents

Total Ca, Fe and S concentrations in the sediments samples were determined on an ICP-OES (Perkin–Elmer Optima 3000) in 1 M HCl (OAE 2 samples) or HNO_3 (PETM samples) solutions in which sample residues were dissolved after digestion in 2.5 mL HF (40%) and 2.5 mL of a $HClO_4$/HNO_3 mixture at 90 °C (left overnight) and subsequent evaporation of the acids at 190 °C. Relative standard deviations for duplicates and in-house standards were <5%. The $CaCO_3$ content in Site 1260 samples was determined by the weight loss after decalcification, assuming all carbonate in the samples is calcite (Forster et al., 2007). The $CaCO_3$ content in samples of the other three sites was calculated from total Ca. The accuracy of the estimation of $CaCO_3$ from total Ca may suffer from the presence of significant clay-bound Ca in $CaCO_3$-poor sediments. Nevertheless, the calculation meets our purpose, which is to differentiate between $CaCO_3$-rich and -poor sediments.

Pyrite content was estimated from the total S or total Fe content of individual samples. Anoxic sediments exposed to atmospheric oxygen are strongly affected by (pyrite) oxidation effects. Detailed Fe and S speciation, as is now commonly used to quantify their pyrite-associated fractions, may therefore fail to provide reliable information on in situ pyrite content. We estimated pyrite contents from total S in the anoxic sections of the investigated profiles with total Fe/total S ratios >0.5, assuming all S is present in pyrite. The assumption is in our view supported by the fact that Fe/S ratios in the investigated anoxic sections of the investigated cores are, in general, relatively close to 0.5, the stoichiometric balance for pyrite, FeS_2. For a small selection of samples of Site 367 with total Fe/total S ratios <0.5, we estimated pyrite contents from total Fe. We are aware of the limitations of this approach and the possibility of an overestimation of the sediment pyrite content. This stems from our assumption that all S or Fe, depending on the Fe/S ratio with respect to FeS_2, is present in pyrite. The amounts of Fe and S available for pyrite formation can deviate considerably from their respective total abundances due to the presence of unreactive Fe and organically bound S. First, there may be a considerable fraction of unreactive silicate–Fe in marine sediments (e.g. Canfield et al., 1996; Raiswell and Canfield, 1998). Importantly, reactive Fe is relatively enriched in sediments under euxinic bottom waters where Fe is scavenged by dissolved sulfide (e.g. Berner and Raiswell, 1983; Lyons and Severmann, 2006). Previous studies have shown that the fraction of Fe that is (highly) reactive towards sulfide in ancient black shales varies between ~0.4 and 0.9 (Shen et al., 2003; März et al., 2008). Secondly, organically-

bound S can be an important sink for S in organic-rich reducing sediments (Böttcher et al., 2006). However, sulfidization of organic matter occurs when S availability exceeds that of reactive Fe for pyrite formation (Passier and De Lange, 1998). Under reducing conditions, most sediment S is indeed present as pyritic S (e.g. Raiswell and Canfield, 1998; Passier et al., 1999; Wijsman et al., 2001). While we acknowledge the limitations associated with this estimation of pyrite contents, we are confident that these do not impact the basic conclusions of our work.

3. RESULTS

Several key geochemical parameters and the P fractionation results are presented in Table 1 and Fig. 1. In general, organic and detrital P account for only minor fractions of total P and show little variation with depth and are therefore not shown. Organic P is low in all OAE 2 sediments (<5% of total P). Detrital P is low (on average <5% of total P) in sediments of sites 367 and 1260 and in the organic-rich layers of the OAE 2 interval of Site 603. Organic and detrital P are higher in the sediments of Site M004A, on average ~25 and 10%, respectively, for the PETM interval, and 10% and 5% for the laminated lower part.

Sediments of Site 367 show alternating $CaCO_3$-rich and -poor layers, while $CaCO_3$ contents at sites 603 and M004A (PETM) are consistently low (<2 wt%). Molar Fe/S ratios are typically above 0.5, except in the OAE 2 interval at Site 367. Pyrite concentrations are elevated in laminated intervals, where molar Fe/S ratios are close to 0.5.

Remarkably high concentrations of exchangeable and Fe-bound P were recorded in the OAE 2 interval of Site 603 and the laminated euxinic lower part of the PETM interval of Site M004A (Table 1 and Fig. 1). For Site 603, Fe-bound P peaks in the intervals that were deposited under strongest oxygen depletion (indicated in Fig. 1 by dark grey bars). The results suggest that the greatest fraction of total P consists of phosphate bound to iron oxyhydroxides in the most anoxic parts of the sediments. Authigenic Ca–P is consistently low in the samples of Site 603 and shows a mirror-image trend with Fe-bound P for site M004A (which for this site includes any exchangeable P that may have been present), with highest concentrations when Fe-bound P is low and vice versa. The same mirror-image trends are recorded for the OAE 2 interval of Site 367, where the P speciation strongly correlates with $CaCO_3$ contents. In $CaCO_3$-rich sediment samples, authigenic Ca-P is the major P phase and Fe-bound P is negligible, while the reverse is recorded when $CaCO_3$ is low.

The relation between $CaCO_3$ content and P fractionation is further demonstrated in Fig. 2. Samples of Site 1260, which all contain >20 wt% $CaCO_3$, show low Fe-bound P and high authigenic Ca–P (see Table 2) while carbonate-poor sediments of site 603 show the opposite: high Fe-bound P and low authigenic Ca–P. A major shift from Fe-bound P as the major P phase to authigenic Ca–P occurs around 4 wt% for the samples of Site 367.

For Site M004A (PETM), $CaCO_3$ content is low in all samples (0.7 wt% on average) and percentages of authigenic Ca–P and Fe-bound P vary strongly (Table 1 and Fig. 3). A small subset of the samples record P fractionation similar to that recorded in the carbonate-poor sediments of sites 367 and 603 (i.e. high Fe-bound P and low authigenic Ca–P). In the M004A samples, strong linear correlations are observed between pyrite content on the one hand and Fe-bound P ($r = 0.81$, $p < 0.05$) and authigenic Ca–P ($r = -0.83$, $p < 0.05$) on the other hand (Fig. 3b). At high pyrite contents, Fe-bound P is by far the dominant phase.

In the samples of Site 367, on average 45% and 20% of total Fe was extracted with CDB (i.e. easily reducible iron oxyhydroxides) and CBA (i.e. poorly crystalline ferric iron oxyhydroxides), respectively (see also Table 1). On average 50% of total Fe in the samples of Site 603 was extracted with CDB. Only a minor fraction of total Fe was extracted with CDB (10–15% on average) or CBA (~5% on average) in the samples of sites 1260 (no CBA data) and M004A.

The molar Fe/P ratios in the CDB and CBA extracts also depend on sediment characteristics (Table 2). For Site 367, CDB Fe/P ratios show a strong positive correlation with $CaCO_3$ contents ($r = 0.88$, $p < 0.05$) with average values around 100 in $CaCO_3$-rich sediments and 15 in $CaCO_3$-poor sediments. Similar values were calculated for the molar Fe/P ratio in CBA extracts. For Site 603, the CDB Fe/P ratio is on average ~50 (~30 in the two laminated organic-rich intervals). For Site M004A (PETM), the CDB Fe/P ratios in the pyrite-rich laminated sediments are significantly lower than in the PETM sediments with lower pyrite contents (13 versus 51). The Fe/P ratios in CBA extracts are similar. The Fe/P ratios in the CDB extracts of Site 1260 samples vary strongly, with the highest CDB Fe/P ratios recorded in the OAE 2 interval.

4. DISCUSSION

4.1. Fe-bound and exchangeable P in anoxic sediments: an artifact of sediment oxidation

The presence of significant amounts of P bound to iron oxyhydroxides in the investigated anoxic sediments with low $CaCO_3$ and high pyrite content points towards alteration of the original P fractionation. The abundance of Fe-bound P increases with degree of oxygen depletion as deduced from proxy evidence. Fe-bound P is high in all $CaCO_3$-poor intervals of Site 367, which experienced anoxic conditions throughout the period during which the investigated section was deposited (Kuypers et al., 2002). For Site 603, Fe-bound P peaks in the black claystone intervals (indicated by the dark grey vertical bars in Fig. 1) characterized by highest C_{org} and redox-sensitive trace metal content and presence of isorenieratene, a biomarker for euxinic conditions in the water column. Also, Fe-bound P is the dominant P phase in the laminated lower part of the PETM interval of Site M004A, which is the most reducing part of the investigated interval with elevated C_{org} and redox-sensitive trace metal content and the presence of isorenieratene (Sluijs et al., 2006, 2008).

In sediments formed under anoxic conditions, reductive dissolution of iron oxyhydroxides and enhanced regeneration of P from organic matter (Ingall et al., 1993; Ingall and Jahnke, 1994) is expected. As a consequence, P in ancient anoxic sediments will predominantly be sequestered

Table 1
Key geochemical parameters and P and Fe fractionation for sites 367, 603, 1260 and M004A. Estimates of pyrite content are only given for samples from laminated, reducing intervals. *Note:* exchP = exchangeable P, FeP = Fe-bound P, Fe_{CDB} = easily reducible ferric Fe, Fe_{CBA} = poorly crystalline ferric Fe.

Depth (mbsf)	$CaCO_3$ (wt%)	Pyrite (wt%)	Fe/S (mol /mol)	Total P (μmol/g)	% exch P	%FeP	% authi P	Total Fe (wt%)	Fe_{CDB}/Fe_{tot}	Fe_{CBA}/Fe_{tot}
Site 367										
637.20	1.4	6.2	0.3	63.9	32.7	65.4	0.9	4.9	0.4	0.4
637.56	14.2	2.5	0.3	37.1	0.1	7.9	89.4	3.4	0.1	0.1
638.09	3.9	4.5	0.4	79.0	15.8	82.3	0.8	5.2	0.5	0.3
638.71	16.6	2.1	0.2	53.2	0.2	3.4	94.6	2.8	0.3	0.1
639.39	0.6	2.7	0.3	13.5	25.7	68.8	1.3	4.0	0.5	0.5
640.11	1.0	1.5	0.3	40.9	2.2	94.5	1.2	2.5	0.3	0.3
640.90	15.0	2.4	0.2	56.1	0.0	5.8	91.7	2.5	0.5	0.1
641.29	3.3	2.1	0.3	32.3	8.1	88.0	1.5	3.2	0.4	0.3
641.71	19.6	1.4	0.3	29.6	0.0	6.1	91.1	2.2	0.8	0.1
642.24	0.9	0.8	1.0	13.4	0.2	90.2	2.1	4.0	0.3	0.0
643.00	21.6	1.3	0.4	47.0	0.0	2.6	92.8	2.2	0.4	0.1
645.93	1.1	0.8	0.7	40.2	0.8	94.8	1.6	3.3	0.3	0.1
646.14	4.1	0.7	0.6	43.9	0.1	10.2	85.7	2.7	0.2	0.1
646.89	1.3	0.7	0.9	30.1	0.7	93.8	1.4	4.0	0.9	0.1
647.93	1.3	0.8	0.6	78.2	0.5	65.0	31.5	2.8	0.5	0.2
649.62	1.6	0.7	0.8	102.4	1.4	95.8	1.5	3.1	0.7	0.2

Depth (mbsf)	$CaCO_3$ (wt%)	Pyrite (wt%)	Fe/S (mol/mol)	Total P (μmol/g)	% exch P	%Fe P	% authi P	Total Fe (wt%)	Fe_{CDB}/Fe_{tot}
Site 603									
1129.99	0.2		0.6	3.1	3.8	45.1	4.4	4.4	0.5
1130.14	0.3	5.3	0.8	32.6	5.1	81.4	3.0	4.1	0.7
1130.21	0.3	5.4	0.7	12.6	1.3	80.9	2.6	3.3	0.7
1130.27	0.3	5.5	0.5	10.5	9.6	77.4	2.2	2.8	0.6
1130.29	0.5	7.5	0.6	12.6	7.2	79.3	2.5	3.9	0.7
1130.37	0.3	4.5	0.5	10.9	4.2	77.2	2.8	2.2	0.5
1130.37	0.5	4.5	0.6	9.3	4.2	82.9	2.2	2.4	0.5
1130.45	0.7	5.4	0.8	9.2	0.3	72.1	3.3	4.1	0.5
1130.47	0.3	4.3	0.9	10.8	1.1	76.3	3.6	3.4	0.5
1130.49	0.5	4.4	1.0	9.9	0.7	72.3	3.8	3.9	0.5
1130.58	0.6		0.8	4.4	0.8	47.1	3.0	5.2	0.4
1130.61	0.4		0.9	4.8	0.7	53.3	2.7	3.9	0.5
1130.62	0.3		0.5	5.8	16.2	64.2	2.5	2.4	0.5
1131.35	1.4		0.6	8.4	5.3	73.7	2.8	6.3	0.2
1131.64	0.6		1.2	11.3	0.3	69.5	3.8	5.3	0.4
1132.12	0.4		1.4	16.6	0.4	82.3	2.4	4.9	0.5
1132.29	0.5	2.8	1.3	15.6	0.7	80.0	3.2	3.3	0.5
1132.43	0.5	4.4	0.8	15.3	1.6	84.9	2.0	3.2	0.7
1132.47	0.4	3.1	0.9	20.4	3.9	90.1	2.6	2.7	0.8
1132.50	0.3	3.2	1.4	18.2	0.9	81.2	3.4	4.2	0.3
1132.56	0.3	2.7	1.3	17.5	3.4	69.7	3.9	3.2	0.4

1132.59	0.3	4.4	0.7	20.3	4.5	84.2	1.9	2.7	0.7
1132.64	0.4	3.9	0.8	26.9	4.2	78.8	3.0	3.0	0.5
1132.69	1.4	4.5	0.7	15.8	1.0	77.2	2.9	3.0	0.5
1132.76	1.1	3.6	1.2	11.3	0.6	71.6	3.6	4.1	0.4
1132.78	0.3	3.3	1.3	8.6	0.8	78.2	4.5	4.1	0.3
1132.82	0.3	3.1	1.2	11.2	0.3	69.7	2.8	3.4	0.4
1132.84	0.5		1.6	12.3	0.6	70.0	3.4	4.2	0.3
1132.87	1.5		1.2	15.8	0.5	63.7	3.1	3.4	0.4
1132.96	0.3		2.1	13.4	0.6	72.7	2.9	3.7	0.3
1134.47	0.3		4.8	14.4	2.5	74.4	4.0	3.5	0.2
1135.12	0.9		4.0	11.0	0.7	59.7	3.9	3.9	0.1

Depth (mcd)	$CaCO_3$ (wt%)	Pyrite (wt%)	Fe/S (mol/mol)	Total P (μmol/g)	%FeP	% Authi P	Total Fe (wt%)	Fe_{CDB}/Fe_{tot}
Site 1260								
422.51	63.2	1.8	0.3	208.9	0.9	94.0	0.8	0.1
423.59	73.8	1.7	0.3	72.7	3.3	96.3	0.8	0.1
423.68	58.8	1.9	0.4	238.9	0.8	97.0	0.9	0.1
423.78	28.7	3.7	0.5	19.2	2.0	95.6	1.7	0.1
424.33	75.5	1.4	0.2	7.1	39.7	52.6	0.7	0.2
424.54	59.2	3.2	0.6	943.8	0.4	72.4	1.5	0.1
424.63	49.8	3.0	0.4	536.7	0.7	93.4	1.4	0.1
424.71	65.9	2.1	0.4	192.1	1.3	94.9	1.0	0.1
424.91	51.9	2.7	0.4	603.1	0.6	86.8	1.2	0.1
425.01	67.5	3.2	0.3	39.1	3.6	95.9	1.5	0.1
425.10	85.7	1.5	0.4	140.0	1.7	96.2	0.7	0.1
425.18	45.9	4.1	0.3	25.5	1.3	97.7	1.9	0.2
425.36	50.1	3.2	0.2	8.9	9.1	86.9	1.5	0.2
425.57	48.2	4.4	0.3	4.4	9.6	86.1	2.0	0.2
425.85	93.9	1.8	0.5	1.6	16.3	74.1	0.8	0.1
426.06	42.4	2.9	0.3	121.2	1.5	96.3	1.4	0.1
426.17	55.7	2.5	0.3	17.5	3.7	91.2	1.1	0.1
426.25	61.0	2.4	0.2	43.0	2.5	94.9	1.1	0.3
426.29	92.6	0.5	0.3	23.2	3.3	93.0	0.2	0.1
426.38	43.0	2.3	0.2	40.3	2.4	95.9	1.1	0.0
426.41	60.7	3.3	0.3	232.7	1.4	97.4	1.5	0.1
426.59	68.7	1.7	0.3	28.1	7.6	91.5	0.8	0.1
426.79	71.3	1.4	0.3	37.8	3.0	95.4	0.7	0.1
426.97	67.7	1.7	0.3	380.7	0.9	98.1	0.8	0.1
427.08	67.4	1.8	0.3	353.2	0.6	98.6	0.8	0.1
427.47	67.5	2.2	0.3	495.7	0.6	95.1	1.0	0.1
428.07	65.5	2.1	0.3	169.6	1.5	98.0	1.0	0.1
428.47	97.6	0.4	0.1	5.1	16.4	82.9	0.2	0.2
429.07	60.5	1.9	0.2	108.2	1.8	96.8	0.9	0.1
429.52	61.2	1.8	0.3	250.1	0.8	91.6	0.8	0.1
430.02	69.4	1.7	0.4	14.9	8.2	88.0	0.8	0.1
430.49	79.4	1.0	0.3	13.6	6.3	90.3	0.4	0.1
431.09	59.8	2.1	0.3	34.3	4.7	92.6	1.0	0.1

(*continued on next page*)

Table 1 (*continued*)

Depth (mcd)	$CaCO_3$ (wt%)	Pyrite (wt%)	Fe/S (mol/mol)	Total P (μmol/g)	%FeP	% Authi P	Total Fe (wt%)	Fe_{CDB}/Fe_{tot}
431.49	56.0	2.6	0.5	209.7	1.4	93.0	1.2	0.1
431.80	54.8	2.4	0.3	70.4	1.6	97.0	1.1	0.1

Depth (mbsf)	$CaCO_3$ (wt%)	Pyrite (wt%)	Fe/S (mol/mol)	Total P (μmol/g)	%FeP	%authi P	Total Fe (wt%)	Fe_{CDB}/Fe_{tot}	Fe_{CBA}/Fe_{tot}
Site M004A									
376.40	0.5		1.5	9.9	13.3	39.5	2.4	0.10	0.06
376.61	0.5		2.1	10.2	11.0	43.6	2.1	0.11	0.06
376.80	0.5		2.1	10.5	11.9	40.0	2.2	0.09	0.06
377.04	0.4		1.1	9.9	15.2	38.6	3.2	0.10	0.06
380.32	0.6		1.7	10.6	4.5	47.0	2.1	0.07	0.06
380.52	0.4	2.1	1.6	9.5	15.2	33.1	3.0	0.08	0.06
380.71	0.4	1.7	1.7	9.2	9.6	38.2	2.7	0.06	0.05
380.93	0.4	2.2	1.4	9.8	8.6	38.5	2.8	0.06	0.05
381.13	0.5	4.5	1.0	11.9	7.0	50.2	4.1	0.06	0.04
381.31	0.4	1.0	2.6	10.7	6.3	45.8	2.4	0.08	0.06
381.53	0.3	1.1	2.3	10.5	11.8	37.3	2.4	0.10	0.06
381.74	0.4	1.7	1.7	10.3	16.0	34.9	2.7	0.10	0.07
381.85	0.5	3.1	1.1	10.5	13.2	39.0	3.3	0.07	0.06
382.02	0.4	3.0	1.2	9.8	16.6	34.6	3.4	0.10	0.05
382.22	0.5	3.5	1.1	10.2	27.5	27.3	3.5	0.14	0.07
382.42	0.5	3.2	1.1	11.5	23.5	32.2	3.4	0.11	0.07
382.62	0.6	8.0	0.7	12.7	41.6	19.0	5.4	0.12	0.07
382.82	0.8	9.2	0.7	28.2	71.1	10.2	6.1	0.17	0.08
383.02	0.7	24.1	0.6	18.1	70.6	8.1	13.1	0.10	0.10
383.22	1.0	24.2	0.6	29.1	84.6	6.2	13.1	0.17	0.11
383.36	1.3	13.7	0.6	52.6	75.2	5.4	7.9	0.21	0.09
383.56	0.8	10.9	0.7	23.2	75.4	8.3	6.7	0.22	0.06
383.76	0.7	11.3	0.6	34.0	77.7	4.5	6.8	0.16	0.09
383.96	1.0	10.7	0.6	17.6	77.1	11.8	6.4	0.21	0.09
384.16	0.7	12.6	0.6	21.0	67.8	7.5	7.3	0.22	0.05
384.37	0.6	12.9	0.6	27.4	80.5	5.2	7.5	0.17	0.06
386.31	0.8	11.8	0.6	23.7	73.9	8.7	6.8	0.15	0.05
386.44	0.8	12.2	0.6	24.3	72.6	6.5	6.9	0.14	0.05
386.61	0.9	12.5	0.6	9.2	14.0	15.7	7.1	0.18	0.04
388.60	0.7		4.4	23.8	4.1	60.9	3.0	0.10	0.06
388.80	0.7		1.1	22.5	3.7	53.5	5.2	0.10	0.04
389.01	0.7		3.4	24.8	7.9	58.4	3.4	0.16	0.05
389.21	0.8		7.0	30.7	9.5	62.6	3.3	0.09	0.05
389.41	1.0		2.3	43.4	3.5	58.1	4.7	0.22	0.07
389.51	0.7		9.6	24.9	9.4	65.0	3.1	0.09	0.05
389.71	0.7		2.7	28.7	4.7	62.9	4.0	0.19	0.07
389.91	0.9		4.8	29.1	3.6	64.8	3.8	0.15	0.07
390.11	0.5		5.3	19.2	8.5	51.6	3.1	0.08	0.04
390.31	0.8		1.7	32.2	4.9	57.0	4.9	0.34	0.07
390.51	0.8		4.4	29.2	4.3	59.3	3.5	0.12	0.06
390.70	0.8		3.8	30.2	4.7	60.9	3.6	0.17	0.12

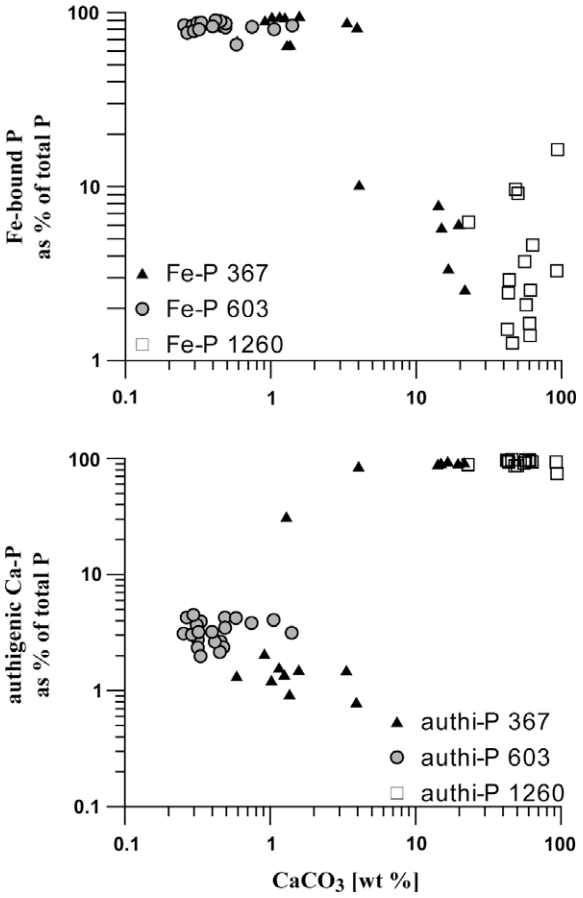

Fig. 2. Fe-bound P and authigenic Ca–P (as % of total P) against $CaCO_3$ contents for sites 367, 603 and 1260 (OAE 2).

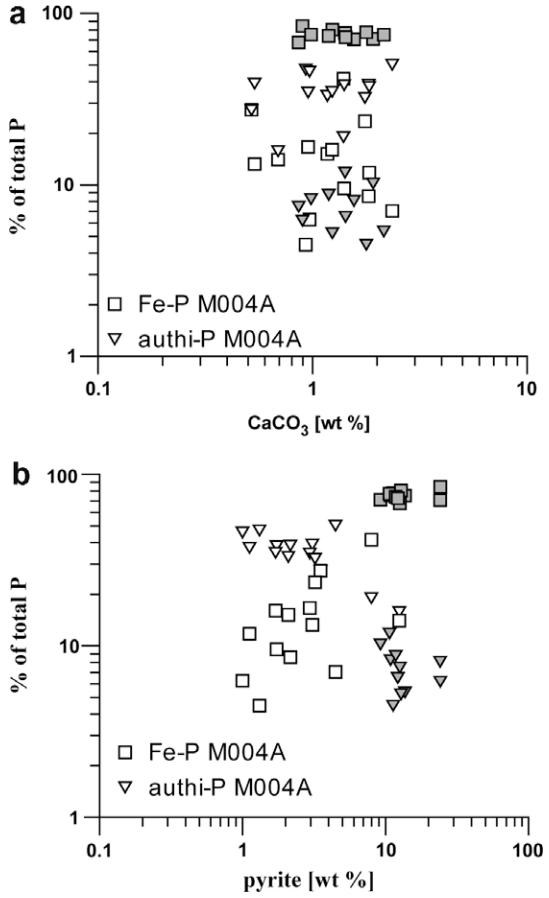

Fig. 3. Fe-bound P and authigenic Ca–P (as % of total P) against $CaCO_3$ (a) and pyrite contents (b) for Site M004A (PETM). Samples with high Fe-bound-P and low authigenic Ca–P at low $CaCO_3$ and relatively high pyrite contents are shown with grey fill.

in calcium phosphate minerals (i.e. authigenic Ca–P). Extensive formation and preservation of redox-sensitive iron oxyhydroxides under strongly reducing conditions over geological time periods is highly unlikely. Reduced Fe-minerals such as vivianite can be excluded given the marine setting and high sulfide contents in the sediments (Selig and Fischer, 2005). Direct sorption of phosphate onto pyrite, proposed as a mechanism for P concentration from sea water on early Earth (Bebié and Schoonen, 1999; De Souza-Barros et al., 2007), is only effective at low pH and low SO_4^{2-} concentrations. These are conditions that did not occur in the marine realm during the Cretaceous and Paleogene. The work of Krom and Berner (1980) confirms that in marine sediments, pyrite has a very low affinity for phosphate.

Oxidation of pyrite during core storage and sample handling provides a plausible mechanism to explain why Fe-bound P, and not authigenic Ca–P, is the dominant P phase in most of the carbonate-poor anoxic sediments with high pyrite contents. Oxygen diffusing into pore water can initiate a process of autocatalytic pyrite oxidation, represented

Table 2
Averaged C_{org}, $CaCO_3$ and pyrite contents, Fe-bound P and authigenic Ca–P phosphorus phases (as percentages of total phosphorus) and Fe/P ratios in CDB and CBA extracts for sites 1260, 603, 367 and M004A. For Site 367, results for high and low carbonate samples are shown separately. For Site M004A, results for high and low pyrite samples are shown separately. Standard deviations from the mean are shown between parentheses.

Site	C_{org} [wt%]	$CaCO_3$ [wt%]	pyrite [wt%]	Fe-bound P [% of total P]	authi P [% of total P]	CDB Fe/P (mol mol^{-1})	CBA Fe/P (mol mol^{-1})
1260 (OAE 2)	9 (±5)	60 (±19)	4 (±2)	5 (±4)	92 (±6)	25 (±47)	n.d.
603 (OAE 2)	5 (±4)	<2	4 (±2)	73 (±11)	3 (±1)	47 (±56)	n.d.
367 (OAE 2) high carbonate	23 (±4)	15 (±6)	2 (±1)	6 (±3)	91 (±3)	101 (±57)	136 (±95)
367 (OAE 2) low carbonate	16 (±12)	<2	2 (±2)	84 (±13)	4 (±10)	14 (±12)	19 (±30)
M004A (PETM) low pyrite	2 (±1)	<2	2 (±1)	13 (±7)	38 (±7)	51 (±38)	63 (±40)
M004A (PETM) high pyrite	3 (±0)	<2	13 (±5)	72 (±11)	9 (±4)	13 (±5)	11 (±8)

by the general reaction pathway (e.g. Hoffmann et al., 1981):

$$FeS_2 + 3.5O_2 + H_2O \rightarrow Fe^{2+} + 2SO_4^{2-} + 2H^+ \quad (1)$$

$$Fe^{2+} + 0.25O_2 + H^+ \rightarrow Fe^{3+} + 0.5H_2O \quad (2)$$

$$FeS_2 + 14Fe^{3+} + 8H_2O \rightarrow 15Fe^{2+} + 2SO_4^{2-} + 16H^+ \quad (3)$$

where ferric iron is thought to be the principal oxidant of pyrite through reaction 3. Reaction 1 characterizes the overall stoichiometry of pyrite oxidation, where oxidation of one mole of pyrite produces two moles of H^+. Thus, oxidation of only a few microgram of pyrite per gram sediment can produce sufficient H^+ to acidify marine pore waters, which have a natural pH of around 8 and make up some 40–60 wt% of marine shales. Apatite dissolution generally increases with decreasing pH. Calculations show that oxidation of less than 1% of the available pyrite in the investigated samples can shift pore water pH from 8 to 4, creating an acidic environment in which apatite is readily dissolved. In fact, a solution with pH 4 is used in the SEDEX procedure to extract authigenic Ca–P in a matter of hours (Ruttenberg, 1992).

Acidic dissolution of 1 mole of fluorapatite requires 12 moles of H^+, following the generalized reaction:

$$Ca_{10}(PO_4)_6F_2 + 12H^+ \rightarrow 10Ca^{2+} + 6H_2PO_4^- + 2F^- \quad (4)$$

Dissolution of carbonate fluorapatite, the common apatite species in marine sediments, where PO_4^{3-} and/or F^- are to a varying extent replaced by CO_3^{2-}, involves a similar dissolution stoichiometry. Dissolution of apatite by H^+ from pyrite oxidation then requires a molar pyrite to apatite ratio of around 6 (12 mol H^+ required per mole apatite, 2 mol H^+ produced per mole pyrite oxidized). The molar pyrite/apatite ratios (with apatite calculated from total P to estimate original sediment apatite content) in the reducing $CaCO_3$-poor sections in the investigated records of sites 367, 603 and M004A are 43, 165 and 330, indicating that more than enough pyrite is present to cause the complete dissolution of apatite upon oxidation in $CaCO_3$-poor sediments. In addition, if we assume that the fraction CDB-extractable Fe of total Fe is a measure for the degree of pyrite oxidation, the averaged molar ratios between oxidized pyrite (calculated as: pyrite content × (Fe extracted with CDB/total Fe)) and total apatite (from total P) are 15, 89 and 55 for the anoxic laminated sections of sites 367, 603 and M004A, respectively. Apparently, enough pyrite is present and oxidized to create and maintain acidic pore waters and theoretically dissolve all sediment apatite. The efficiency of apatite dissolution of course depends on the distribution of pyrite and apatite in the sediments. The acid produced by pyrite oxidation can further affect the chemistry of exposed anoxic sediments, for instance through $CaCO_3$ dissolution and subsequent gypsum ($CaSO_4$) formation (Wiggering, 1993). Visible gypsum was present on the cores from Site M004A, Site 603 and, most notably, Site 367.

The ferrous iron that is released during pyrite oxidation (reaction 1) and subsequently converted to ferric Fe (reaction 2) will in part precipitate as Fe oxyhydroxides. The formation of oxyhydroxides can be enhanced in oxygenated (micro)environments, where buffering of H^+ by acidic dissolution of apatite or other sediment constituents (e.g. silicates) has resulted in recovery of pH to more neutral values. Under such conditions, the ferrous iron released by pyrite oxidation will react to form iron (oxy)hydroxide through (e.g. Kleinmann et al., 1981; Bigham et al., 1990):

$$Fe^{2+} + 2.5H_2O + 0.25O_2 \rightarrow Fe(OH)_3 + 2H^+ \quad (5)$$

The formation of iron oxyhydroxides from ferrous iron and subsequent adsorption of the phosphate released by acidic apatite dissolution will lead to an increase in the fraction of Fe-bound, and possibly exchangeable, P. The occurrence of exchangeable P, which is most abundant in the sediments of Site 367, is likely dependent on the ratio between Fe and P released by pyrite oxidation and apatite dissolution. Site 367 sediments are characterized by relatively low Fe (pyrite) and high P content (Table 1 and Fig. 1). For this site, the abundant P released by apatite dissolution is not all incorporated in or strongly bound to iron oxyhydroxides, resulting in the presence of phosphate that is only loosely adsorbed onto sediment components such as iron oxyhydroxides.

The low molar Fe/P ratios of the (poorly crystalline) iron oxyhydroxides extracted with CDB and CBA from the organic-rich, carbonate-poor anoxic sections of sites 367 and M004A (Table 2) indicate that these are relatively freshly formed. Fresh, amorphous iron oxyhydroxides have a much higher P adsorption capacity than their crystalline successors (Slomp et al., 1996b). The higher Fe/P ratios in extracts of Site 603 samples are the result of the low abundance of P in these samples, which upon pyrite oxidation has led to the formation of iron oxyhydroxides with only little associated P. Labile (amorphous) iron oxyhydroxides will likely not be preserved in sediments for ~90 Myrs, but will become more crystalline or dissolve. The occurrence of fresh iron oxyhydroxides corroborates the hypothesis that the extracted Fe-bound P is predominantly an artifact of exposing anoxic sediment to atmospheric oxygen after sediment recovery from the sea floor. This is further supported by the fact that the presence of Fe-bound P in the investigated samples depends on the availability of pyrite in the sediment. A clear concurrent drop of pyrite contents and Fe-bound P as a percentage of total P was observed in the sediments from the later stages of the PETM (above 383 m, Table 1 and Fig. 1).

4.2. $CaCO_3$ as a buffer against changes in P fractionation upon pyrite oxidation

Whether apatite is dissolved by the acid produced from pyrite oxidation depends on the $CaCO_3$ content of the sediments, allowing the reaction:

$$CaCO_3 + H^+ \rightarrow Ca^{2+} + HCO_3^-. \quad (6)$$

As $CaCO_3$ is orders of magnitude more sensitive to acidic dissolution than apatite (Amankonah et al., 1985; Ruben and Bennett, 1987) it can effectively buffer acidity and shield apatite from dissolution in calcareous sediments. This shielding effect is demonstrated in the sediments of Site

367. Here, authigenic Ca–P seems largely unaffected in samples with $CaCO_3$ contents >4 wt%, while in carbonate-poor samples nearly all authigenic Ca–P is converted to Fe-bound P and, to a lesser extent, exchangeable P (Table 1 and Fig. 1). Furthermore, results of Site 1260 samples with overall high $CaCO_3$ contents (average 60 wt%) showed low Fe-bound P contents (on average <1 μmol/g, equivalent to <5% of total P) in sediments that were deposited under severe anoxia and contained visible pyrite (Erbacher et al., 2004; Brumsack, 2006).

Reactions 1 and 6 show that for complete buffering by $CaCO_3$ of the acidity produced through pyrite oxidation, a $CaCO_3$ to pyrite molar ratio of 2 or higher is required. Molar ratios between $CaCO_3$ and oxidized pyrite above 2 are only observed in the samples of Site 1260 (>400 on average) and the carbonate-rich samples of Site 367 (~25 on average). Note, however, that the oxidation of pyrite and subsequent carbonate or apatite dissolution likely occurs in micro-environments in the sediments and thus strongly depends on the spatial distribution of pyrite, apatite and carbonate. For instance, our results show that even when enough pyrite was oxidized to dissolve all apatite, varying (small) amounts of authigenic Ca–P were present in the investigated sediments. Sediment heterogeneity limits the predictability of oxidation artifacts from bulk geochemical parameters. It therefore cannot be ruled out that formation of Fe-bound P through acidic dissolution of apatite can occur in carbonate-rich anoxic sediments that have been exposed to oxygen.

4.3. Implications of altered P fractionation in anoxic sediments exposed to oxygen

The alteration of P fractionation as a result of sediment oxidation seriously hampers an accurate reconstruction of marine P cycling and bottom water conditions from the distribution of sedimentary P phases in the geological record. The proposed mechanism provides a simple explanation for the puzzling occurrence of abundant Fe-bound P in anoxic sediments, where previous authors could not explain this observation or invoked changes in bottom water redox conditions to account for it.

For example, März et al. (2008) found abundant Fe-bound P (up to ~50% of total P) in organic-rich sediments with relatively low $CaCO_3$ and elevated C_{org} and S content deposited during the Coniacian–Santonian oceanic anoxic event and attributed this to preservation of Fe-bound P in the sediment under anoxic, non-sulfidic bottom waters. We propose that post-recovery formation of Fe-bound P in these reducing sediments is likely the major source of this Fe-bound P. Clearly, caution must be taken when linking bottom water redox conditions to P fractionation in such reducing sediments. It is noteworthy that the $CaCO_3$ content in the black shale layer drops from ~60 outside the layer to ~25 wt%, supporting our suggestion that the post-recovery formation of Fe-bound P is not necessarily restricted to carbonate-poor sediments but depends on oxidized microenvironments in the sediment.

While they do not comment on the P fractionation measured in sediments from around the OAE 2 interval at several locations, Mort et al. (2007) found Fe-bound P to increase at the onset of OAE 2 in outcrop sediments from Manilva (Spain). In the C_{org}-rich and carbonate-poor OAE 2 interval, up to 80% of total P is Fe-bound P, while only ~15% of total P is Fe-bound P prior to the OAE 2 interval. Abundant Fe-bound P with increasing anoxia is unlikely, unless we assume the Fe-bound P is an artifact of pyrite oxidation. A second outcrop site with a carbonate-poor OAE 2 interval, Furlo (Italy), showed a contrasting record with low Fe-bound P and authigenic Ca-P as the major P reservoir in the black shale section. Local conditions apparently exert strong control on the extent to which P speciation can be affected by oxidation. In general, in situ Fe-bound P formation under anoxic conditions is probably overestimated due to the presence of artifact Fe-bound P. This precludes an accurate understanding of the sensitivity of the Fe-bound P reservoir to changes in bottom water oxygenation. It can also lead to incorrect assumptions regarding bottom water conditions based on P fractionation data.

Post-recovery alteration of P fractionation may not only distort the original signal of redox control on sediment P fractionation, but also may hinder an accurate understanding of P transformations during sediment burial. For example, Filippelli (2001) measured significant Fe-bound P (between ~15% and 40% of total P) in cores of ~60 m with carbonate-poor anoxic sediments from Saanich Inlet. The nature of the iron oxyhydroxides remained unclear. The author used the decrease of Fe-bound P with depth and mirror-image trends of Fe-bound P and authigenic Ca–P as evidence for sink switching between these two reservoirs. While we do not contest the author's basic conclusions regarding P cycling mechanisms, the size of the Fe-bound P reservoir and the rate of P transformations may have been misrepresented by the presence of artifact Fe-bound P. The cores represent a ~10,000-yr depositional history, and the P fractionation may wrongfully lead to the conclusion that P associated with easily reducible iron oxyhydroxides is an important long-term P sink in reducing sediments. On a broader scale, neglecting post-recovery alterations of P fractionation may affect current estimates of global P burial budgets. Our results indicate that the importance of Fe-bound P as a long-term P sink on a global scale, estimated at ~20% of total P by Ruttenberg (1993), might be an overestimation.

In this study, strong alteration of the P fractionation was observed in the relatively fresh, pyrite-rich sediments of Site M004A (drilled in 2004, sampled in 2006). This indicates that pyrite oxidation and Fe-bound P formation can occur on short timescales, and not only in sediments stored for decades (sites 367 and 603). Lukkari et al. (2007) showed that within months, significant changes in P speciation occurred in carbonate-poor sediments from the Baltic Sea that were exposed to oxygen. These findings suggest that only analysis of samples that have been shielded from oxygen since recovery can provide unambiguous information on the in situ P fractionation in carbonate-poor reducing sediments.

4.4. Recommendations for sediment storage

To preserve the geochemical signature of an anoxic depositional setting, not only for P, Fe and S, but also for many other redox-sensitive elements, shielding from oxygen is vital. Two methods can be used to preserve sediments after recovery: freezing and/or anoxic storage. Freezing will strongly reduce the oxygen penetration into the pore water and sediment. For small-scale expeditions, slicing sediments in an oxygen-free environment (e.g. in a glovebox flushed with an inert gas such as N_2 or Ar) and storing short cores and samples at −20 °C (preferably oxygen-free) is recommended, feasible and already applied by various researchers. We realize that for larger expeditions, such as undertaken by the IODP, immediate processing of samples or anoxic frozen storage of thousands of meters of core is unrealistic. We propose that immediately after core recovery sub samples from organic-rich, reducing intervals are taken and stored frozen, preferably in an oxygen-free environment (e.g. in gas-tight vessels or bags). Several grams per sample could already suffice for determination of the organic and inorganic geochemistry. We recommend that subsequent chemical characterization of redox-sensitive elements occurs in an oxygen-free environment (i.e. a glovebox). If frozen storage is not feasible, directly removing the pore water by freeze-drying samples under vacuum will likely slow down oxidation of the sediment.

5. CONCLUSIONS

Pyrite oxidation in anoxic sediments exposed to atmospheric oxygen can lead to extensive conversion of authigenic Ca–P to Fe-bound and exchangeable P. The acid produced by pyrite oxidation dissolves Ca–P minerals, and the released P is bound in freshly formed iron oxyhydroxides. The extent to which these conversions can take place is controlled by the abundance of pyrite (source of acid and iron oxyhydroxides) and $CaCO_3$, which can effectively shield Ca–P minerals from dissolution.

The conversion of Ca–P to Fe-bound P seriously hampers a meaningful reconstruction from the geological record of P burial and cycling mechanisms and bottom water conditions during formation of (ancient) anoxic sediments. Up to now, the effects of sediment oxidation on P fractionation have been largely overlooked. Instead, the occurrence of Fe-bound P in supposedly anoxic sediments has (likely wrongly) been attributed to variations in bottom water oxygenation, and in situ formation or preservation of Fe–P minerals.

Besides affecting P fractionation, oxidation effects may strongly affect a variety of elements and minerals in anoxic sediments that are sensitive to either oxidation (e.g. metal sulfides) or acidic dissolution (e.g. $CaCO_3$).

To minimize these oxidation effects, we recommend frozen storage of carefully sealed sediment samples and, if possible, cores. Sediment sampling and chemical characterization of redox-sensitive elements should preferably be performed in an oxygen-free environment, such as a glovebox.

ACKNOWLEDGMENTS

This research used samples and data provided by the DSDP and (I)ODP. We thank W. Hale and A. Wülbers (IODP Bremen Core Repository) for core handling. R. Knoop is thanked for sediment analyses at Utrecht University. The Netherlands Organisation for Scientific Research is acknowledged for financial support to P. Kraal and C.P. Slomp (NWO-VIDI grant 864.05.004) and A. Sluijs (NWO-VENI grant 863.05.004). Timothy Lyons, Karl Föllmi, Albert Colman and an anonymous reviewer are thanked for their valuable comments that improved the quality of this paper.

REFERENCES

Amankonah J. O., Somasundaran P. and Ananthapadmabhan K. P. (1985) Effects of dissolved mineral species on the dissolution/precipitation characteristics of calcite and apatite. *Colloids and Surfaces* **15**, 295–307.

Anschutz P., Zhong S. J., Sundby B., Mucci A. and Gobeil C. (1998) Burial efficiency of phosphorus and the geochemistry of iron in continental margin sediments. *Limnology and Oceanography* **43**, 53–64.

Backman, J., Moran, K., McInroy, D.B., Mayer, L.A. and the Expedition 302 Scientists, 2006. In *Proc. IODP, 302*. Integrated Ocean Drilling Program Management International, Inc., Edinburgh.

Bebié J. and Schoonen M. A. A. (1999) Pyrite and phosphate in anoxia and an origin-of-life hypothesis. *Earth and Planetary Science Letters* **171**, 1–5.

Berner R. A. and Raiswell R. (1983) Burial of organic carbon and pyrite sulfur in sediments over phanerozoic time: a new theory. *Geochimica et Cosmochimica Acta* **47**, 855–862.

Bigham J. M., Schwertmann U., Carlson L. and Murad E. (1990) A poorly crystallized oxyhydroxysulfate of iron formed by bacterial oxidation of Fe(II) in acid mine waters. *Geochimica et Cosmochimica Acta* **54**, 2743–2758.

Böttcher, M.E., Hetzel, A., Brumsack, H.-J., Schipper, A., (2006). Sulfur-iron-carbon geochemistry in sediments of the Demerara Rise. In *Proc. ODP, Sci. Results 207*. (eds. D.C. Mosher, J. Erbacher and M.J. Malone): Ocean Drilling Program, College Station, TX, pp. 1–23.

Brumsack H. J. (2006) The trace metal content of recent organic carbon-rich sediments: Implications for Cretaceous black shale formation. *Palaeogeography Palaeoclimatology Palaeoecology* **232**, 344–361.

Canfield D. E., Lyons T. W. and Raiswell R. (1996) A model for iron deposition to euxinic Black Sea sediments. *American Journal of Science* **296**, 818–834.

Chi R., Xiao C. and Gao H. (2006) Bioleaching of phosphorus from rock phosphate containing pyrites by *Acidithiobacillus ferrooxidans*. *Minerals Engineering* **19**, 979–981.

De Souza-Barros F., Braz-Levigard R., Ching-San Y., Monte M., Bonapace J., Montezano V. and Vieyra A. (2007) Phosphate sorption and desorption on pyrite in primitive aqueous scenarios: relevance of acidic → alkaline transitions. *Origins of Life and Evolution of Biospheres* **37**, 27–45.

Erbacher, J., Mosher, D.C., Malone, M.J., et al., 2004. Proc. ODP, Init. Repts. 207: College Station, TX (Ocean Drilling Program).

Filippelli G. M. (2001) Carbon and phosphorus cycling in anoxic sediments of the Saanich Inlet, British Columbia. *Marine Geology* **174**, 307–321.

Forster A., Schouten S., Moriya K., Wilson P. A. and Sinninghe Damsté J. S. S. (2007) Tropical warming and intermittent

cooling during the Cenomanian/Turonian oceanic anoxic event 2: sea surface temperature records from the equatorial Atlantic. *Paleoceanography* **22**, 1–14.

Friedrich O. and Erbacher J. (2006) Benthic foraminiferal assemblages from Demerara Rise (ODP Leg 207, western tropical Atlantic): possible evidence for a progressive opening of the Equatorial Atlantic Gateway. *Cretaceous Research* **27**, 377–397.

Hoffmann M. R., Faust B. C., Panda F. A., Koo H. H. and Tsuchiya H. M. (1981) Kinetics of the removal of iron pyrite from coal by microbial catalysis. *Applied and Environmental Microbiology* **42**, 259–271.

Holland H. D. (1978) *The Chemistry of the Atmosphere and Oceans*. John Wiley and Sons, New York.

Hyacinthe C., Bonneville S. and Van Cappellen P. (2006) Reactive iron(III) in sediments: chemical versus microbial extractions. *Geochimica et Cosmochimica Acta* **70**, 4166–4180.

Imhoff J. F. (1995) Taxonomy and physiology of phototrophic purple bacteria and green sulfur bacteria. In *Anoxygenic Photosynthetic Bacteria* (eds. R. E. Blankenship, M. T. Madigan and C. E. Bauer). Springer, Berlin.

Ingall E. and Jahnke R. (1994) Evidence for enhanced phosphorus regeneration from marine sediments overlain by oxygen depleted waters. *Geochimica et Cosmochimica Acta* **58**, 2571–2575.

Ingall E. D., Bustin R. M. and Van Cappellen P. (1993) Influence of water column anoxia on the burial and preservation of carbon and phosphorus in marine shales. *Geochimica et Cosmochimica Acta* **57**, 303–316.

Kleinmann R. L. P., Crerar D. A. and Pacelli R. R. (1981) Biogeochemistry of acid mine drainage and a method to control acid formation. *Minerals Engineering* **33**, 300–306.

Krom M. D. and Berner R. A. (1980) Adsorption of phosphate in anoxic marine sediments. *Limnology and Oceanography* **25**, 797–806.

Kuypers M. M. M., Pancost R. D., Nijenhuis I. A. and Sinninghe Damsté J. S. (2002) Enhanced productivity led to increased organic carbon burial in the euxinic North Atlantic basin during the late Cenomanian oceanic anoxic event. *Paleoceanography* **17**, 1051.

Kuypers M. M. M., Lourens L. J., Rijpstra W. R. C., Pancost R. D., Nijenhuis I. A. and Sinninghe Damsté J. S. (2004a) Orbital forcing of organic carbon burial in the proto-North Atlantic during oceanic anoxic event 2. *Earth and Planetary Science Letters* **228**, 465–482.

Kuypers M. M. M., van Breugel Y., Schouten S., Erba E. and Sinninghe Damsté J. S. S. (2004b) N_2-fixing cyanobacteria supplied nutrient N for Cretaceous oceanic anoxic events. *Geology* **32**, 853–856.

Lancelot, Y., Seibold, E., et al., 1977. Init. Repts. DSDP 41. Washington (US Government Printing Office).

Lucotte M. and d'Anglejan B. (1985) A comparison of several methods for the determination of iron hydroxides and associated orthophosphates in estuarine particulate matter. *Chemical Geology* **48**, 257–264.

Lukkari K., Leivuori M. and Hartikainen H. (2007) Fractionation of sediment phosphorus revisited: II. Changes in phosphorus fractions during sampling and storing in the presence or absence of oxygen. *Limnology and Oceanography: Methods* **5**, 445–456.

Lyons T. W. and Severmann S. (2006) A critical look at iron paleoredox proxies: new insights from modern euxinic marine basins. *Geochimica et Cosmochimica Acta* **70**, 5698–5722.

März C., Poulton S. W., Beckmann B., Küster K., Wagner T. and Kasten S. (2008) Redox sensitivity of P cycling during marine black shale formation – dynamics of sulfidic and anoxic, non-sulfidic bottom waters. *Geochimica et Cosmochimica* **72**, 3703–3717.

Mort H. P., Adatte T., Föllmi K. B., Keller G., Steinmann P., Matera V., Berner Z. and Stüben D. (2007) Phosphorus and the roles of productivity and nutrient recycling during oceanic anoxic event 2. *Geology* **35**, 483–486.

Ohtsubo M. (1995) Oxidation of pyrite in marine clays and zinc adsorption. In *Dredging, Remediation and Containment of Contaminated Sediments* (eds. K. D. Demars, G. N. Richardson, R. N. Yong and R. C. Chaney). American Society for Testing and Materials, Philadelphia.

Passier H. F., Middelburg J. J., de Lange G. J. and Böttcher M. E. (1999) Modes of sapropel formation in the eastern Mediterranean: some constraints based on pyrite properties. *Marine Geology* **153**, 199–219.

Passier H. F. and De Lange G. J. (1998) Sedimentary sulfur and iron chemistry in relation to the formation of Eastern Mediterranean sapropels. *Proceedings of the Ocean Drilling Program, Scientific Results* **160**, 249–259.

Peterson G. S., Ankley G. T. and Leonard E. N. (1996) Effect of bioturbation on metal-sulfide oxidation in surficial freshwater sediments. *Environmental Toxicology and Chemistry* **15**, 2147–2155.

Raiswell R. and Canfield D. E. (1998) Sources of iron for pyrite formation in marine sediments. *American Journal of Science* **298**, 219–245.

Ruben J. A. and Bennett A. A. (1987) The evolution of bone. *Evolution* **41**, 1187–1197.

Ruttenberg K. C. (1992) Development of a sequential extraction method for different forms of phosphorus in marine sediments. *Limnology and Oceanography* **37**, 1460–1482.

Ruttenberg K. C. (1993) Reassessment of the oceanic residence time of phosphorus. *Chemical Geology* **107**, 405–409.

Sageman B. B., Meyers S. R. and Arthur M. A. (2006) Orbital time scale and new C-isotope record for Cenomanian–Turonian boundary stratotype. *Geology* **34**, 125–128.

Schenau S. J. and De Lange G. J. (2000) A novel chemical method to quantify fish debris in marine sediments. *Limnology and Oceanography* **45**, 963–971.

Schlanger S. O. and Jenkyns H. C. (1976) Cretaceous oceanic anoxic events: causes and consequences. *Geologie en Mijnbouw* **55**, 179–184.

Selig U. and Fischer K. (2005) Phosphorus accumulation in lake sediments during the last 14, 000 years: Description by fractionation techniques and X-ray micro-analysis. *Journal of Freshwater Ecology* **20**, 347–359.

Sinninghe Damsté J. S., Wakeham S. G., Kohnen M. E. L., Hayes J. M. and De Leeuw J. W. (1993) A 6, 000-year sedimentary molecular record of chemocline excursions in the Black Sea. *Nature* **362**, 827–829.

Shen Y., Knoll A. H. and Walter M. R. (2003) Evidence for low sulphate and anoxia in a mid-Proterozoic marine basin. *Nature* **423**, 632–635.

Slomp C. P., Epping E. H. G., Helder W. and Van Raaphorst W. (1996a) A key role for iron-bound phosphorus in authigenic apatite formation in North Atlantic continental platform sediments. *Journal of Marine Research* **54**, 1179–1205.

Slomp C. P., Van der Gaast S. J. and Van Raaphorst W. (1996b) Phosphorus binding by poorly crystalline iron oxides in North Sea sediments. *Marine Chemistry* **52**, 55–73.

Slomp C. P., Thomson J. and De Lange G. J. (2002) Enhanced regeneration of phosphorus during formation of the most recent eastern Mediterranean sapropel (S1). *Geochimica et Cosmochimica Acta* **66**, 1171–1184.

Sluijs A., Bowen G. J., Brinkhuis H., Lourens L. J. and Thomas E. (2007) The Palaeocene–Eocene thermal maximum super green-

house: biotic and geochemical signatures, age models and mechanisms of global change. In *Deep Time Perspectives on Climate Change: Marrying the Signal from Computer Models and Biological Proxies* (eds. M. Williams, A. M. Haywood, A. J. Gregory and D. N. Schmidt). The Micropalaeontological Society, Special Publications, The Geological Society London, London.

Sluijs, A., Röhl, U., Schouten, S., Brumsack, H.-J., Sangiorgi, F., Sinninghe Damsté, J.S., Brinkhuis, H., 2008. Arctic late Paleocene–early Eocene paleoenvironments with special emphasis on the Paleocene-Eocene thermal maximum (Lomonosov Ridge, Integrated Ocean Drilling Program Expedition 302). *Paleoceanography* 23, PA1S11, doi:10.1029/2007PA001495.

Sluijs A., Schouten S., Pagani M., Woltering M., Brinkhuis H., Sinninghe Damsté J. S., Dickens G. R., Huber M., Reichart G.-J., Stein R., Matthiessen J., Lourens L. J., Pedentchouk N., Backman J. and Moran K.and the Expedition 302 Scientists (2006) Subtropical Arctic Ocean temperatures during the Palaeocene/Eocene thermal maximum. *Nature* **441**, 610–613.

Stookey L. L. (1970) Ferrozine – a new spectrophotometric reagent for iron. *Analytical Chemistry* **42**, 779–781.

Strickland, J.D., Parsons, T.R., 1972. A practical handbook of seawater analysis. *Bulletin* 167, Fisheries Research Board of Canada.

Tamburini F., Huon S., Steinmann P., Grousset F. E., Adatte T. and Föllmi K. B. (2002) Dysaerobic conditions during Heinrich events 4 and 5: evidence from phosphorus distribution in a North Atlantic deep-sea core. *Geochimica et Cosmochimica Acta* **66**, 4069–4083.

Tyrrell T. (1999) The relative influences of nitrogen and phosphorus on oceanic primary production. *Nature* **400**, 525–531.

Van Cappellen P. and Ingall E. D. (1994) Benthic phosphorus regeneration, net primary production, and ocean anoxia – a model of the coupled marine biogeochemical cycles of carbon and phosphorus. *Paleoceanography* **9**, 677–692.

Van Hinte, J.E., Wise, S.W., Jr., et al., 1984. Init. Repts. DSDP 93. Washington (US Govt. Printing Office).

Wiggering H. (1993) Sulfide oxidation – an environmental problem within colliery spoil dumps. *Environmental Geology* **22**, 99–105.

Wijsman J. W. M., Middelburg J. J., Herman P. M. J., Böttcher M. E. and Heip C. H. R. (2001) Sulfur and iron speciation in surface sediments along the northwestern margin of the Black Sea. *Marine Chemistry* **74**, 261–278.

Zachos J., Lohmann K. C., Walker J. C. G. and Wise, Jr., S. W. (1993) Abrupt climate change and transient climates during the Palaeogene: a marine perspective. *Journal of Geology* **101**, 191–213.

Associate editor: Timothy W. Lyons